Published: ApJ, December 1, 2000
Preprint typeset using LaTeX style emulateapj v. 04/03/99

EXPECTATIONS FOR AN INTERFEROMETRIC SUNYAEV-ZEL'DOVICH EFFECT SURVEY FOR GALAXY CLUSTERS

Gilbert P. Holder [1], Joseph J. Mohr [1,2,3], John E. Carlstrom [1], August E. Evrard [4]
Erik M. Leitch [1]

Published: ApJ, December 1, 2000

ABSTRACT

We estimate the expected yield of a non-targeted survey for galaxy clusters using the Sunyaev-Zel'dovich effect (SZE). Estimating survey yields requires a detailed model for both cluster properties and the survey strategy. We address this by making mock observations of galaxy clusters in cosmological hydrodynamical simulations. The mock observatory consists of an interferometric array of ten 2.5 m diameter telescopes, operating at a central frequency of 30 GHz with a bandwidth of 8 GHz. For a survey covering 1 deg^2/month, we find that clusters with a mass above $2.5 \times 10^{14} h_{50}^{-1} M_\odot$ will be detected at any redshift, with the exact limit showing a modest redshift dependence.

Using a Press-Schechter prescription for evolving the number densities of clusters with redshift, we determine that such a survey should find hundreds of galaxy clusters per year, many at high redshifts and relatively low mass – an important regime uniquely accessible to SZE surveys. Currently favored cosmological models predict ~ 25 clusters per square degree.

Subject headings: cosmology:theory — galaxies: clusters: general — large-scale structure of universe

1. INTRODUCTION

The evolution of the cluster abundance is a sensitive probe of the mass density Ω_m (e.g., Viana and Liddle 1999, Bahcall and Fan 1998, Oukbir, Bartlett, and Blanchard 1997). X-ray cluster surveys have started to constrain Ω_m, but they are limited by their sample size and rapid decline in sensitivity with redshift, making the counts very sensitive to the selection function. While the selection function is presumably well-understood, it would be preferable to have a probe whose sensitivity does not fall off precipitously with redshift. We will show that a Sunyaev-Zel'dovich effect survey is ideal in this regard.

Hot ionized cluster gas interacts with passing cosmic microwave background (CMB) photons, distorting the CMB spectrum to create a decrement of CMB flux at lower frequencies and an excess at higher frequencies. This spectral distortion is independent of the redshift of the cluster, and only depends on the optical depth to Compton scattering and the temperature of the gas. This is the thermal Sunyaev-Zel'dovich effect (SZE) (Sunyaev and Zel'dovich 1972).

There have been several previous predictions of the number of clusters expected in SZE surveys (e.g., Bartlett and Silk 1994, Barbosa *et al.* 1996), with most earlier work focusing on the total SZE flux. As survey yields depend sensitively on the observing strategy, we focus here on yields for a proposed interferometric survey (see Mohr *et al.* 1999).

A large catalog of high-redshift clusters that extends to low masses would be an extremely useful resource for several reasons. Observations suggest that the universe may no longer be matter-dominated, with a large fraction ($\sim 70\%$) of its present energy density either in the form of curvature (open universe) or vacuum (cosmological constant) energy. Linear theory suggests that structure formation will slow considerably when the expansion dynamics are no longer dominated by matter; this occurred around $z \lesssim 1.5$ if current measurements of Ω_m are correct. Therefore, the cluster abundance out to $z \sim 2$ should be a valuable probe of the matter density of the universe.

A large collection of high-redshift, low-mass clusters also would provide an ideal sample for exploring evolution of the intra-cluster medium (ICM) and feedback from galaxy formation. The shallow potential wells of less massive clusters are more strongly affected by energy input from non-gravitational sources and are therefore the best place to search for the signatures of such processes.

Estimating the cluster yield for an SZE survey requires that we know which properties of a cluster determine its likelihood of detection. We will show that the mass of a cluster is the single most important factor in determining if a given cluster can be detected by an interferometric survey. In this case, the calculation of the expected yield separates into two distinct exercises: finding the minimum observable mass as a function of redshift and calculating the number density of clusters above a given mass threshold as a function of redshift.

We determine the minimum observable mass as a function of redshift by making synthetic observations of N-body+gas hydrodynamical simulations (§2). The number density of clusters is calculated using the Press-Schechter prescription (Press and Schechter 1974; §3). Section 4 contains estimates of the expected survey yield and the results are discussed in Section 5.

[1]Department of Astronomy and Astrophysics, University of Chicago, 5640 S. Ellis Ave., Chicago, IL 60637
[2]Chandra Fellow
[3]Departments of Astronomy and Physics, University of Illinois, 1002 West Green Street, Urbana, IL 61801
[4]Department of Physics, University of Michigan, Ann Arbor, MI 48109

2. CLUSTER DETECTABILITY

The SZE decrement along a given line-of-sight is independent of cosmology. It is simply proportional to the integrated thermal pressure along the line-of-sight and therefore only depends on the properties of the cluster. The decrement can be written

$$\frac{\Delta T}{T_{CMB}} = g(x) \int dl\, n_e(l) \frac{k_B T_e(l)}{m_e c^2} \sigma_T, \qquad (1)$$

where n_e is the electron number density, T_e is the electron temperature, m_e is the electron rest mass, σ_T is the Thomson cross section, $g(x) = x(e^x+1)/(e^x-1) - 4$ with $x = h\nu/k_B T_{CMB}$ and the integral is along the entire line-of-sight; by assumption, the only significant contribution to the integral comes from the cluster atmosphere. In the Rayleigh-Jeans limit ($\nu \ll 200$ GHz) the dimensionless frequency factor $g(x) = -2$.

The specific intensity S_ν in the Rayleigh-Jeans regime is $S_\nu = 2k_B \Delta T \nu^2/c^2 d\Omega$, where $d\Omega$ is the effective solid angle of the observations. Thus the total SZE flux decrement S_{tot} for a galaxy cluster can be written

$$S_{tot}(z) = \frac{2k_B^2 \nu^2 g(x) \sigma_T T_{CMB}}{m_e c^4 d_A(z)^2} \langle T_e \rangle_n \frac{M_{200} f_{ICM}}{\mu_e m_p}, \qquad (2)$$

where $d_A(z)$ is the angular diameter distance, $\langle T_e \rangle_n$ is the electron density weighted mean temperature in the cluster, μ_e is the mean molecular weight per electron, m_p is the proton mass, f_{ICM} is the ratio of total gas mass to binding mass, and M_{200} is a measure of the cluster virial mass, defined as the mass within r_{200}, the radius where the mean interior density is 200 times the critical density. Note that we explicitly ignore contributions to the SZE flux coming from outside the virial region.

Equation 2 indicates that the total SZE flux for a cluster is directly proportional to the cluster virial mass; the only dependence on cluster structure is through the density weighted mean temperature $\langle T_e \rangle_n$. This is unique to a survey with a beam large enough that the cluster SZE is not resolved. However, for maximum brightness sensitivity to the SZE effect, the beam used for a survey should be well matched to the typical angular scale subtended by clusters. Such a survey will partially resolve most of the clusters and will therefore be somewhat sensitive to the internal cluster structure. We show below that for a population of clusters with similar ICM mass fraction f_{ICM} and similar temperature structure, the detection threshold for an interferometric SZE survey is also effectively a virial mass limit.

2.1. *Mock Interferometric SZE Observations*

We determine the detection threshold of an SZE survey by analyzing mock observations of numerical cluster simulations. These mock observations are appropriate for a proposed ten-element interferometer, composed of 2.5 m diameter telescopes outfitted with receivers operating at a central frequency of 30 GHz and a bandwidth of 8 GHz. We assume a correlator efficiency of 0.88 and an aperture efficiency of 0.77. We take the system temperature below the atmosphere to be 21 K; this includes contributions from spillover past the primary. We assume an atmospheric column with opacity $\tau = 0.045$ at zenith, which is a conservative estimate appropriate for a low altitude, moderately dry site such as the Owens Valley Radio Observatory in summer. The integration time on each cluster is 42 hr, composed of six 7 hr tracks on the cluster. This exposure on each piece of the sky would allow us to survey $\sim$1 deg^2 per month.

Interferometers measure the visibility, $V(u,v)$ which is the Fourier transform of the sky brightness distribution multiplied by the primary beam of the telescopes. We create mock observations at a redshift z by imaging hydrodynamical cluster simulations (described in detail below) at that redshift; we place those clusters at the appropriate angular diameter distance, multiply the resulting SZE image with the primary beam of the 2.5 m dishes (modeled as a Gaussian with $FWHM = 14.7'$ at 30 GHz), and then Fourier transform to produce visibilities $V(u,v)$. We then sample these visibilities at the same locations in u–v space which appear in our simulated 7 hr array track and add the appropriate noise.

2.2. *Hydrodynamical Cluster Simulations*

The effects of ongoing cluster merging on the ICM density and temperature structure can be calculated self-consistently in hydrodynamical simulations. Therefore, these simulations provide a way of producing test clusters whose complexity approaches that of observed clusters. In this work we use an ensemble of 36 hydrodynamical cluster simulations carried out within three different cold dark matter (CDM) dominated cosmologies (1) SCDM ($\Omega_m = 1$, $\sigma_8 = 0.6$, $h_{50} = 1$, $\Gamma = 0.5$), (2) OCDM ($\Omega_m = 0.3$, $\sigma_8 = 1.0$, $h_{50} = 1.6$, $\Gamma = 0.24$), and (3) LCDM ($\Omega_m = 0.3$, $\Omega_\Lambda = 0.7$, $\sigma_8 = 1.0$, $h_{50} = 1.6$, $\Gamma = 0.24$). Here σ_8 is the power spectrum normalization on $8h^{-1}$ Mpc scales; initial conditions are Gaussian random fields consistent with a CDM transfer function with the specified Γ (Davis *et al.* 1985). These simulations have been used previously for studies of the X-ray emission from galaxy clusters (Mohr and Evrard 1997, Mohr, Mathiesen, and Evrard 1999).

Within each cosmological model, we use two 128^3 N–body only simulations of cubic regions with scale $\sim$ 400 Mpc to determine sites of cluster formation. Within these initial runs the virial regions of clusters with Coma–like masses of 10^{15} M$_\odot$ contain $\sim 10^3$ particles.

Using the N–body results for each model, we choose clusters for additional study, resimulating them at higher resolution with gas dynamics and gravity, as described below. The size of the resimulated region is set by the turnaround radius for the enclosed cluster mass at the present epoch. The large wavelength modes of the initial density field are sampled from the initial conditions of the large scale N–body simulations, and power on smaller scales is sampled from the appropriate CDM power spectrum. The simulation scheme is P3MSPH (Evrard 1988), the ICM mass fraction is fixed at $f_{ICM} = 0.2$, and radiative cooling and heat conduction are ignored.

The high resolution, hydrodynamical simulations of individual clusters require two steps: (1) an initial, 32^3, purely N–body simulation to identify which portions of the initial density field lie within the cluster virial region at the present epoch, and (2) a final 64^3, three species, hydrodynamical simulation. In the final simulation, the

portion of the initial density field which ends up within the cluster virial region by the present epoch is represented using dark matter and gas particles of equal number (with mass ratio 4:1), while the portions of the initial density field that do not end up within the cluster virial region by the present epoch are represented using a third, collisionless, high mass, species. The high mass species is 8 times more massive than the dark matter particles in the central, high resolution region. This approach allows us to include the tidal effects of the surrounding large scale structure and the gas dynamics of the cluster virial region with simulations that take only a few days of CPU time on a low end UltraSparc.

The scale of the simulated region surrounding each cluster is in the range 50–100 Mpc, and varies as $M_{halo}^{1/3}$, where M_{halo} is approximately the mass enclosed within the present epoch turnaround radius. Thus, the 36 simulated clusters in our final sample have similar fractional mass resolution; the spatial resolution varies from 125–250 kpc. We will find that the clusters of greatest interest to us are those with mass $\gtrsim 2 \times 10^{14} M_{\odot}$, which have at least several thousand gas particles, even in the lowest resolution simulations (i.e., the highest mass at $z = 0$). The masses of the final cluster sample vary by an order of magnitude. Following procedures described in Evrard (1990), we create SZE decrement images along three orthogonal lines of sight for each cluster. Each image is 128^2 and spans a distance of $6.7 h_{50}^{-1}$ Mpc in the cluster rest frame.

A strength of using numerical cluster simulations is that structural evolution consistent with the cosmological model is accounted for naturally by simply examining higher redshift outputs of the simulations.

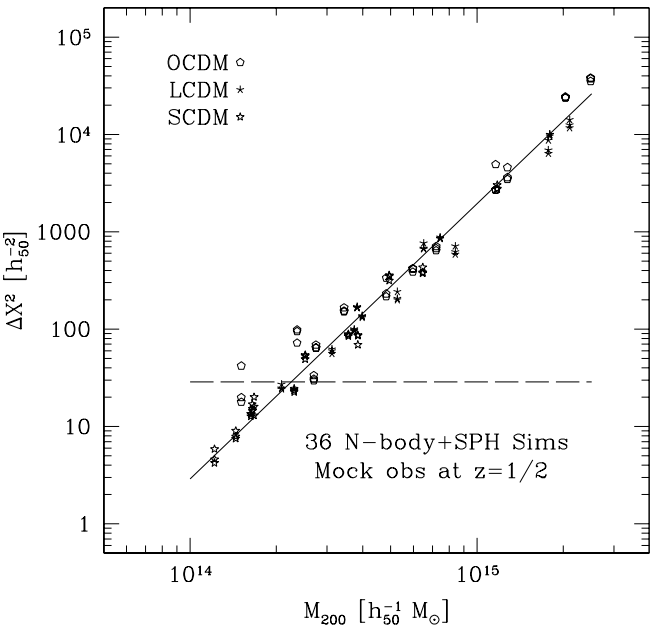

FIG. 1.— Detection significance, $\Delta\chi^2$ relative to null model, as a function of cluster mass for an interferometric SZE survey. All clusters were imaged at a distance corresponding to z=0.5 in an $\Omega_m = 0.3$ and $\Omega_\Lambda = 0.7$ universe. The dashed horizontal line corresponds to a 5σ detection for a two-parameter fit.

2.3. *Determining the Survey Detection Threshold*

We attempt to detect the clusters in the mock observations by fitting the data to the Fourier transforms of spherical β models (Cavaliere and Fusco-Femiano 1978), with $\beta = 4/3$. The results are not sensitive to the value of β, and in fact a simple Gaussian works well. We choose this value of β because its transform is a simple exponential and because the best fits to the SZE decrement images from the simulations yield a mean value $\langle\beta\rangle = 1.1$. We determine the best fit core radius θ_c and central decrement ΔT_o by minimizing χ^2; the $\Delta\chi^2$ difference between the best fit β model and the null model (no cluster present) provides a measure of the significance of the cluster detection. We set our threshold $\Delta\chi^2 > 28.7$ (5σ for two degrees of freedom).

Figure 1 shows the detection significance for 108 mock observations of the simulated clusters output at redshift $z = 0.5$. Observations of clusters in all three cosmologies appear on the same plot, and for this example we have imaged all the clusters at the same angular diameter distance and accounted for differences in $H_\circ$. There is a striking correlation between the detection significance and cluster virial mass, indicating that even when complex cluster dynamics are considered, the survey detection threshold can still be effectively described as a mass threshold. The scatter about this correlation is a reflection of the variation in cluster structure due to different merger histories and projection effects. We determine the mass threshold by examining the $\Delta\chi^2$-M_{200} relation and determining the virial mass at which $\Delta\chi^2 = 28.7$. We calculate the RMS scatter about the relation at $\Delta\chi^2 > 28.7$, and use that scatter as an estimate of the width of the detection threshold in mass; the number of mock observations used to characterize the RMS varies between 21 in our highest redshift bin to over 100 in our low redshift bins. We model the scatter as a Gaussian distribution in χ^2 at each mass. In this way, the fraction of detected clusters at each mass is expressed as an integral over a Gaussian.

Note that the small scatter about the $\Delta\chi^2$-M_{200} relation indicates that mass is indeed the primary factor in determining cluster detectability. Moreover, the fact that all three cosmologies produce consistent relations once differences in H_o are accounted for indicates the relative insensitivity of the detection threshold to differences in cluster structure.

By repeating this exercise at several redshifts, we determine the survey mass threshold as a function of redshift, shown in Figure 2. Note that the thresholds differ for each cosmology because of differences in the angular diameter distance- redshift relation $d_A(z)$. The error bars on the mass limit points indicate the RMS scatter in mass about the $\Delta\chi^2 - M_{200}$ relations (see Fig. 1).

The hydrodynamical simulations cannot be used to extract mass thresholds beyond redshift $z \sim 2.3$, because no clusters in our ensemble are massive enough to lie above the detection threshold. For higher redshift and to aid in interpolating the mass threshold at arbitrary redshift, we use mock observations of spherical β models normalized to agree with the simulations (curves in Figure 2). We evolve the β-models in redshift using the spherical collapse model (Lahav et al. 1991); this evolution is self-similar, accounting for the difference in cluster structure due to evolution of the mean cosmological density. We use these smooth curves essentially as fitting functions.

The insensitivity to redshift of the minimum detectable mass in an interferometric survey follows from a balancing of several effects. The increasing angular diameter distance d_A with redshift decreases the total cluster SZE flux as d_A^{-2} (see equation 2), tending to increase our limiting mass. However, this effect is largely offset by cluster evolution. At higher redshifts clusters are denser, and, at constant virial mass M_{200}, have higher virial temperatures T. Both of these effects increase the total SZE flux. In addition, at higher redshift a cluster has a smaller apparent size, which enhances the cluster visibility $V(u,v)$ (Fourier transform of SZE decrement distribution; see §2.1) at the baselines where we make our measurements. Taken together, these effects largely explain the behavior of the limiting mass with redshift.

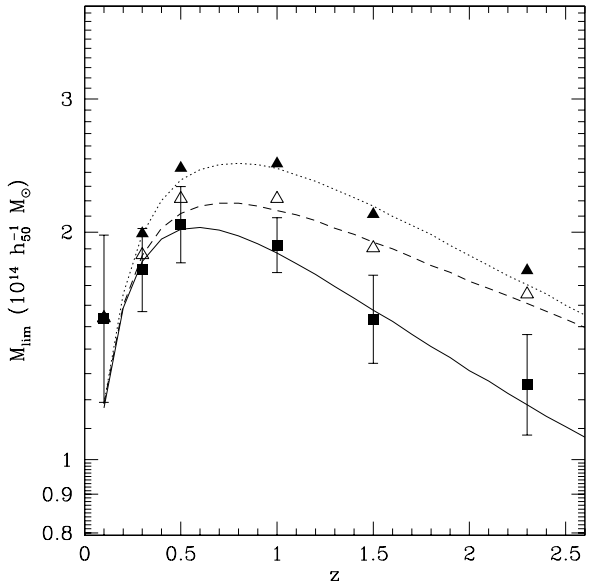

FIG. 2.— Mass thresholds of detection from the simulations for our three canonical cosmologies. The differences in mass thresholds between cosmologies are simply showing the cosmological dependence of the angular diameter distance–redshift relation. From top to bottom, results are shown for ΛCDM (solid triangles and dotted line), oCDM (open triangles and dashed line) and τCDM (solid squares and solid line). The uncertainties in the mass threshold are the same for all cosmologies but, for clarity, are only shown for the τCDM points.

3. THE CLUSTER ABUNDANCE AND ITS REDSHIFT EVOLUTION

Given a minimum observable mass, one can calculate the number of observed clusters as:

$$N(M > M_{thres}) = c \int d\Omega \int dz \int_{M_{thres}(z)}^{\infty} dM \, \frac{dn(M,z)}{dM} \frac{d_A(z)^2(1+z)^2}{H(z)} \quad , \quad (3)$$

where $d\Omega$ is the solid angle and $n(M,z)$ is the comoving number density. To calculate the comoving number density of clusters, we used the Press-Schechter prescription (Press and Schechter 1974).

The comoving number density of bound objects between masses M and $M+dM$ at redshift z is given by

$$\frac{dn(M,z)}{dM} = -\sqrt{\frac{2}{\pi}} \frac{\overline{\rho}}{M} \frac{d\sigma(M,z)}{dM} \frac{\delta_c}{\sigma^2(M,z)} \exp\left[\frac{-\delta_c^2}{2\sigma^2(M,z)}\right] \quad , \quad (4)$$

where $\overline{\rho}$ is the mean comoving background density, $\sigma(M,z)$ is the variance of the fluctuation spectrum filtered on mass scale M, and δ_c is the effective linear overdensity of a perturbation which has collapsed and virialized. In principle, δ_c has a modest dependence on the cosmological density parameter; the spherical collapse model predicts a variation of only $\sim 5\%$ for $\Omega_m \sim 0.1 - 1$. In this work, we assume a constant threshold $\delta_c = 1.69$ for simplicity (Peebles 1980).

Following Viana and Liddle (1999), we take the variance in spheres of radius R to be

$$\sigma(R,z) = \sigma_8(z) \Big(\frac{R}{8h^{-1}Mpc} \Big)^{-\gamma(R)} , \quad (5)$$

where

$$\gamma(R) = (0.3\Gamma + 0.2) \left[2.92 + \log_{10} \Big(\frac{R}{8h^{-1}Mpc} \Big) \right] . \quad (6)$$

The comoving radius R is determined as the radius which contains mass M at the current epoch, while Γ is the usual CDM shape parameter, taken to be 0.25 for this study (Peacock and Dodds 1994, Dodelson and Gaztanaga 1999) unless stated otherwise; we show that the results are insensitive to the exact choice of Γ.

We examine the cluster abundance in three cosmological models: oCDM ($\Omega_m = 0.3, \Omega_\Lambda = 0, h = 0.65, \Gamma = 0.25, \sigma_8 = 1.0$), ΛCDM ($\Omega_m = 0.3, \Omega_\Lambda = 0.7, h = 0.65, \Gamma = 0.25, \sigma_8 = 1.0$), and τCDM ($\Omega_m = 1, \Omega_\Lambda = 0, h = 0.5, \Gamma = 0.25, \sigma_8 = 0.56$), with the last model simply a CDM model with the transfer function modified to agree with observations of galaxy clustering. Note that these models differ slightly from the cosmologies assumed for the simulations.

All models are chosen to have a global ICM fraction $f_{ICM} = 0.2$, in rough agreement with observed ICM mass fractions of clusters (David, Jones, and Forman 1995, White and Fabian 1995, Grego *et al.* 2000, Mohr, Mathiesen, and Evrard 1999). As can be seen from equation 2, the mass limits will depend on the ICM mass fraction and therefore the expected yields will also be sensitive to f_{ICM}.

We show that the expected survey yield is very sensitive to σ_8, also calculating the expected yields for oCDM with a lower value of $\sigma_8 = 0.85$ (e.g., Viana and Liddle 1999). The constraints on σ_8 will improve dramatically in the near future, as new X-ray telescopes are expected to provide a much better determination of the local abundance, so we do not expect uncertainties in σ_8 to affect interpretation of survey results.

In a critical density universe ($\Omega_m = 1, \Omega_\Lambda = 0$), $\sigma_8 \propto (1+z)^{-1}$. Following Carroll, Press, and Turner (1992), we express growth in alternate cosmologies through a growth suppression factor which can be approximated as

$$g(\Omega_m, \Omega_\Lambda) = \frac{5}{2} \frac{\Omega_m}{\left[\Omega_m^{4/7} - \Omega_\Lambda + \Big(1 + \Omega_m/2\Big)\Big(1 + \Omega_\Lambda/70\Big) \right]} \quad . \quad (7)$$

In this notation, we can now express the normalization of the power spectrum as

$$\sigma_8(z) = \frac{\sigma_8(0)}{1+z} \frac{g(\Omega_m(z), \Omega_\Lambda(z))}{g(\Omega_m(0), \Omega_\Lambda(0))} \quad . \quad (8)$$

4. EXPECTED SURVEY YIELD

Figure 3 shows both the differential counts as a function of redshift and integrated number of clusters for our three cosmologies. Cluster physics is especially uncertain at high redshift, so we have chosen to cut off all integrals at a redshift of $z = 4$.

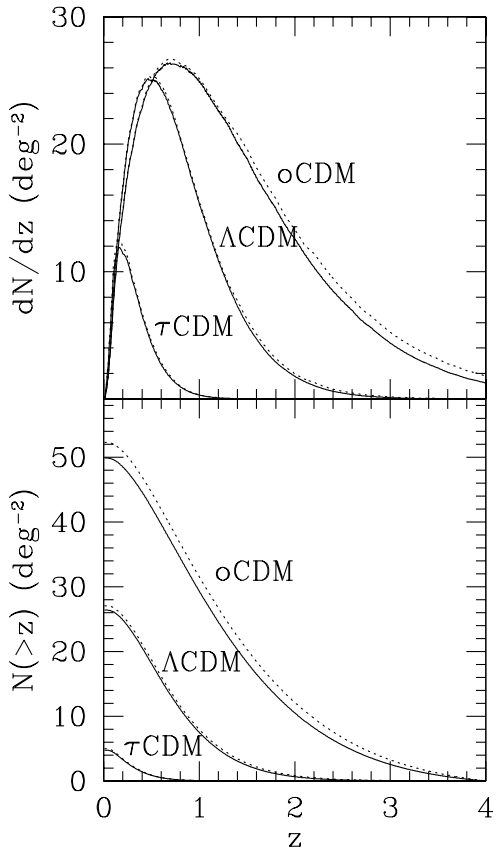

FIG. 3.— Differential counts (top panel) and integrated counts (bottom) as a function of redshift per square degree for two different methods of dealing with the limiting mass. The solid curve for each cosmology assumes a step function at the best fit limit, while the dotted curve corresponds to a Gaussian distribution of χ^2 at each mass.

These results are quite exciting, because they indicate that an SZE survey will yield a large cluster catalog extending to high redshift. If the currently favored ΛCDM model is correct, then we expect to detect 300 clusters in a one year survey. Figure 3 also shows that the width of the mass limit has little effect on the cluster yield. The yield for each cosmology is shown with two curves; the solid curve corresponds to a step function mass limit where $\Delta\chi^2 = 28.7$, and the dashed curve corresponds to a mass limit modeled as a Gaussian probability distribution in $\Delta\chi^2$ at each mass, with variance set by the scatter around the $\Delta\chi^2 - M_{200}$ relation seen in the mock observations. In particular, the largest differences arise mainly in the high-redshift region, where there are few clusters above our mass threshold. While encouraging, this threshold uncertainty requires more attention before future SZE surveys can be correctly interpreted.

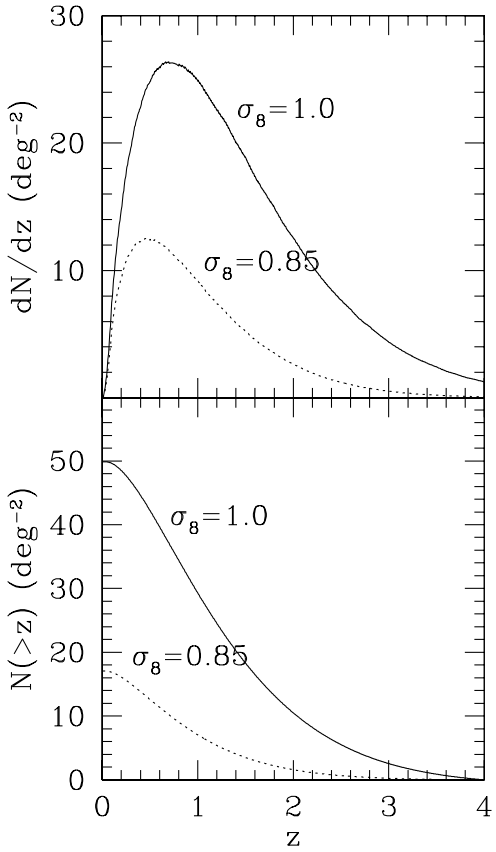

FIG. 4.— Differential (top panel) and integrated (bottom) expected number of cluster in an oCDM model for two values of the normalization of the power spectrum, $\sigma_8 = 0.85$ (dotted) and 1.0 (solid).

The differences between cosmologies at $z \gtrsim 1$ are very promising. Differences arise because of the different rates of structure growth, the dependence of the mass threshold on the angular diameter distance, and the differences in the volume element of the survey. Open models have both a smaller angular diameter distance and more structure at high redshift, both leading to more observed clusters. The effect of ΛCDM probing a larger volume is a relatively small effect.

The expected cluster yield depends on cosmology through the growth rate of perturbations (fixed mainly by the density parameter Ω_m), the volume per unit solid angle and redshift, and the shape and normalization of the initial power spectrum. Varying Γ, the CDM shape parameter, within the 95% confidence interval, $0.2 < \Gamma < 0.3$ (Peacock and Dodds 1994, Dodelson and Gaztanaga 1999), leads to increases ($\Gamma = 0.3$) or decreases ($\Gamma = 0.2$) in the integrated counts of 6% for ΛCDM, 8% for oCDM and 17% for τCDM. The effect is small, indicating that SZE survey counts alone will not strongly constrain the shape of the power spectrum. However, cluster samples constructed through SZE surveys can be used to study the shape of the power spectrum through other means, such as the two-point correlation function.

On the other hand, the normalization of the power spectrum, parameterized by σ_8, is quite important for predicted SZE counts, as demonstrated in Figure 4. For clarity, we have only shown the effect for oCDM. The uncer-

tainty in σ_8 results in a large uncertainty in the cluster yield. Upcoming X-ray observations of nearby clusters are expected to constrain σ_8 to much higher accuracy, and the proposed SZE survey will provide an independent measurement. Thus, while the σ_8 uncertainty is significant for predicting yields, it will not be a serious impediment to interpreting results from an SZE survey. It is important to note that, even for low values of σ_8, we expect to find a significant number of high-redshift clusters.

5. DISCUSSION

In a low-density universe, half of the clusters in an SZE survey will have $z \gtrsim 1$. While other surveys may yield comparable numbers of clusters at high redshift by surveying a larger fraction of the sky, the SZE catalog will be unique in having similar sensitivity at all redshifts; SZE surveys are effectively limited only by the abundance of clusters above the lowest observable mass. PLANCK is expected to find $\sim 10^4$ clusters, but the effective limiting mass is fairly high, resulting in relatively few high-redshift clusters (De Luca, Desert, and Puget 1995, da Silva *et al.* 1999).

An interferometric survey with a synthesized beam that partially resolves clusters has several advantages. Point sources are easily identified and removed from the data; thus, it is unlikely that point sources will systematically affect the magnitude of the observed cluster decrement. In addition, the more massive clusters in our sample can be imaged with high S/N at the same time as they are detected.

Extensive follow-up will be required to make best use of an SZE survey. Extensive optical observations will be required to obtain redshifts for the detected clusters. This may be difficult for the highest-redshift objects, but it is not an insurmountable problem. Follow-up with X-ray telescopes would be helpful as well, but the low-mass, high-redshift objects are expected to be undetectable in the X-ray band, even with $10^5 s$ XMM exposures. However, redshifts, ICM temperatures and X-ray images for a portion of the sample would enable direct SZE+X-ray distances, such as those being measured with the currently available data (Reese *et al.* 1999 and references therein). These distances constrain the angular diameter distance relation, which provides an independent measurement of the cosmological matter density; these results would be complementary to those available from consideration of the cluster counts alone.

Deep exposures such as the ones considered here could be contaminated by primary anisotropies in the CMB. A minimum separation of 2.5m corresponds to multipole $\ell = 1571$ at 30 GHz. At this scale, the CMB anisotropy levels could well be larger than $10\mu K$, which would be above the noise levels that we have assumed but well below the detection threshold. A shift to higher ℓ may be required to avoid these effects, which can be achieved by longer baselines (which could allow larger telescopes) or a higher observing frequency. We have found that a shift to $\ell \sim 3000$ can be easily accommodated with only a small loss in cluster detection efficiency. The most numerous clusters will be the low-mass clusters near the detection threshold, which will be the most compact. Because of this, moving to higher multipoles would not severely affect our sensitivity to these objects, while this would decrease possible CMB contamination significantly. Indeed, larger telescopes may even be slightly more efficient for detecting high-redshift low-mass clusters, as the smaller primary beam is better matched to the compact nature of these objects.

We use an ICM mass fraction of 20% in these simulations, which is inconsistent with the observational constraints, $f_{ICM} = 0.21 h_{50}^{-1.5}$ (Mohr, Mathiesen, and Evrard 1999, Grego *et al.* 2000), if $H_\circ$ is significantly higher than 50 $\mathrm{km\,s^{-1}Mpc^{-1}}$. However, simple virial arguments ($T \propto M^{2/3}$) and Eqn. 2 indicate that the limiting mass scales as $f_{ICM}^{0.6}$. For $H_\circ = 80\,\mathrm{km\,s^{-1}Mpc^{-1}}$, we expect $f_{ICM} = 0.10$. While a gas fraction of only 10% would seriously reduce the expected number of clusters (by a factor of 2.5-3) the resulting catalog would still be large and unique.

An uncertainty that we have not discussed is the effect of galaxy formation or preheating on the ICM structure and SZE detectability. While this is being addressed with numerical simulations currently in progress, we do not believe that our results should depend significantly on gas evolution. ICM evolution mainly affects the core regions of clusters (Ponman, Cannon, and Navarro 1999), on angular scales smaller than those for which the brightness sensitivity of the interferometer is optimized, 2' to 7'. The total SZE flux from the unresolved core depends only on the temperature and the number of electrons at that temperature (see §2). Even fairly extreme models of gas evolution lead to only small changes in the expected counts for a survey sensitive primarily to total SZE flux (Holder and Carlstrom 1999) and we expect this to be true for any survey that does not resolve the core regions of clusters.

While the expected cluster yield should be fairly insensitive to ICM evolution, the properties of the cluster sample and their evolution with redshift will shed considerable light on the question of evolution of the ICM. At the same time, such a survey will provide determinations of key cosmological parameters that will be entirely independent of all other determinations.

We are indebted to Erik Reese for his efforts in developing some of the code that was used for this analysis. This is work supported by NASA LTSA grant number NAG5-7986. JEC acknowledges support from the David and Lucile Packard Foundation and a NSF-YI grant. GPH is supported by the DOE at Chicago and Fermilab. JJM is supported through Chandra Fellowship grant PF8-1003, awarded through the Chandra Science Center. The Chandra Science Center is operated by the Smithsonian Astrophysical Observatory for NASA under contract NAS8-39073. AEE acknowledges support from NSF AST-9803199 and NASA NAG5-8458.

REFERENCES

Bahcall, N. and Fan, X. 1998, ApJ, 504, 1.
Barbosa, D., Bartlett, J., Blanchard, A., and Oukbir, J. 1996, A&A, 314, 13.
Bartlett, J. G. and Silk, J. 1994, ApJ, 423, 12.
Carroll, S., Press, W., and Turner, E. 1992, ARA&A, 30, 499.
Cavaliere, A. and Fusco-Femiano, R. 1978, A&A, 70, 677.
da Silva, A., Barbosa, D., Liddle, A., and Thomas, P. 1999, MNRAS, submitted, (astro–ph/9906289).
David, L., Jones, C., and Forman, W. 1995, ApJ, 445, 578.
Davis, M., Efstathiou, G., Frenk, C. S., and White, S. D. M. 1985, ApJ, 292, 371.
De Luca, A., Desert, F. X., and Puget, J. L. 1995, A&A, 300, 335.
Dodelson, S. and Gaztanaga, E. 2000, MNRAS, 312, 774.
Evrard, A. E. 1988, MNRAS, 235, 911.
Evrard, A. E. 1990, ApJ, 363, 349.
Grego, L., Carlstrom, J. E., Reese, E. D., Holder, G. P., Holzapfel, W L., Joy, M. K., Mohr, J. J., and Patel, S. 2000, ApJ, in press.
Holder, G. and Carlstrom, J. 1999, in Microwave Foregrounds, ed. A. de Oliveira-Costa and M. Tegmark, (San Francisco:ASP), 199 .
Lahav, O., Rees, M.J., Lilje, P. B., and Primack, J.R. 1991, MNRAS, 251, 128 .
Mohr, J., and Evrard, A. E. 1997, ApJ, 491, 38.
Mohr, J., Carlstrom, J., Holder, G., Holzapfel, W., Joy, M., Leitch, E., and Reese, E. 1999, in From Extrasolar Planets to Cosmology: the VLT Opening Symposium, ed. J. Bergeron and A. Renzini, (Berlin: Springer-Verlag), 150.
Mohr, J., Mathiesen, B., and Evrard, A. E. 1999, ApJ, 517, 627.
Oukbir, J., Bartlett, J. G., and Blanchard, A. 1997, A&A, 320, 365.
Peacock, J. and Dodds, S. 1994, MNRAS, 267, 1020.
Peebles, P. 1980. *The Large Scale Structure of the Universe*. Princeton University Press, Princeton.
Ponman, T. J., Cannon, D. B., and Navarro, J. F. 1999, Nature, 397, 135.
Press, W. and Schechter, P. 1974, ApJ, 187, 425.
Reese, E. D. *et al.* 2000, ApJ, 533, 38.
Sunyaev, R. and Zel'dovich, Y. 1972, Comments Astrophys. Space Phys., 4, 173.
Viana, P. and Liddle, A. 1999, MNRAS, 303, 535.
White, D. A. and Fabian, A. C. 1995, MNRAS, 273, 72.